Hindawi Publishing Corporation
EURASIP Journal on Advances in Signal Processing
Volume 2007, Article ID 95281, 17 pages
doi:10.1155/2007/95281

Research Article

Low-Complexity Geometry-Based MIMO Channel Simulation

Florian Kaltenberger,[1] Thomas Zemen,[2] and Christoph W. Ueberhuber[3]

[1] *Austrian Research Centers GmbH (ARC), Donau-City-Strasse 1, 1220 Vienna, Austria*
[2] *ftw. Forschungszentrum Telekommunikation Wien, Donau-City-Strasse 1, 1220 Vienna, Austria*
[3] *Institute for Analysis and Scientific Computing, Vienna University of Technology, Wiedner Hauptstrasse 8-10/101, 1040 Vienna, Austria*

Received 30 September 2006; Revised 9 February 2007; Accepted 18 May 2007

Recommended by Marc Moonen

The simulation of electromagnetic wave propagation in time-variant wideband multiple-input multiple-output mobile radio channels using a geometry-based channel model (GCM) is computationally expensive. Due to multipath propagation, a large number of complex exponentials must be evaluated and summed up. We present a low-complexity algorithm for the implementation of a GCM on a hardware channel simulator. Our algorithm takes advantage of the limited numerical precision of the channel simulator by using a truncated subspace representation of the channel transfer function based on multidimensional discrete prolate spheroidal (DPS) sequences. The DPS subspace representation offers two advantages. Firstly, only a small subspace dimension is required to achieve the numerical accuracy of the hardware channel simulator. Secondly, the computational complexity of the subspace representation is *independent* of the number of multipath components (MPCs). Moreover, we present an algorithm for the projection of each MPC onto the DPS subspace in $\mathcal{O}(1)$ operations. Thus the computational complexity of the DPS subspace algorithm compared to a conventional implementation is reduced by more than one order of magnitude on a hardware channel simulator with 14-bit precision.

1. INTRODUCTION

In mobile radio channels, electromagnetic waves propagate from the transmitter to the receiver via multiple paths. A geometry-based channel model (GCM) assumes that every multipath component (MPC) can be modeled as a plane wave, mathematically represented by a complex exponential function. The computer simulation of time-variant wideband multiple-input multiple-output (MIMO) channels based on a GCM is computationally expensive, since a large number of complex exponential functions must be evaluated and summed up.

This paper presents a novel low-complexity algorithm for the computation of a GCM on hardware channel simulators. Hardware channel simulators [1–5] allow one to simulate mobile radio channels in real time. They consist of a powerful baseband signal processing unit and radio frequency frontends for input and output. In the baseband processing unit, two basic operations are performed. Firstly, the channel impulse response is calculated according to the GCM. Secondly, the transmit signal is convolved with the channel impulse response. The processing power of the baseband unit limits the number of MPCs that can be calculated and hence the model accuracy. We note that the accuracy of the channel simulator is limited by the arithmetic precision of the baseband unit as well as the resolution of the analog/digital converters. On the ARC SmartSim channel simulator [2], for example, the baseband processing hardware uses 16-bit fixed-point processors and an analog/digital converter with 14-bit precision. This corresponds to a maximum achievable accuracy of $E_{\max} = 2^{-13}$.

The new simulation algorithm presented in this paper takes advantage of the limited numerical accuracy of hardware channel simulators by using a truncated basis expansion of the channel transfer function. The basis expansion is based on the fact that wireless fading channels are highly oversampled. Index-limited snapshots of the sampled fading process span a subspace of small dimension. The same subspace is also spanned by index-limited discrete prolate spheroidal (DPS) sequences [6]. In this paper, we show that the projection of the channel transfer function onto the DPS subspace can be calculated approximately but very efficiently

in $\mathcal{O}(1)$ operations from the MPC parameters given by the model. Furthermore, the subspace representation is independent of the number of MPCs. Thus, in the hardware simulation of wireless communication channels, the number of paths can be increased and more realistic models can be computed. By adjusting the dimension of the subspace, the approximation error can be made smaller than the numerical precision given by the hardware, allowing one to trade accuracy for efficiency. Using multidimensional DPS sequences, the DPS subspace representation can also be extended to simulate time-variant wideband MIMO channel models.

One particular application of the new algorithm is the simulation of Rayleigh fading processes using Clarke's [7] channel model. Clarke's model for time-variant frequency-flat single-input single-output (SISO) channels assumes that the angles of arrival (AoAs) of the MPCs are uniformly distributed. Jakes [8] proposed a simplified version of this model by assuming that the number of MPCs is a multiple of four and that the AoAs are spaced equidistantly. Jakes' model reduces the computational complexity of Clarke's model by a factor of four by exploiting the symmetry of the AoA distribution. However, the second-order statistics of Jakes' simplification do not match the ones of Clarke's model [9] and Jakes' model is not wide-sense stationary [10]. Attempts to improve the second-order statistics while keeping the reduced complexity of Jakes' model are reported in [6, 9–14]. However, due to the equidistant spacing of the AoAs, none of these models achieves all the desirable statistical properties of Clarke's reference model [15]. Our new approach presented in this paper allows us to reduce the complexity of Clarke's original model by more than an order of magnitude without imposing any restrictions on the AoAs.

Contributions of the paper

(i) We apply the DPS subspace representation to derive a low-complexity algorithm for the computation of the GCM.
(ii) We introduce approximate DPS wave functions to calculate the projection onto the subspace in $\mathcal{O}(1)$ operations.
(iii) We provide a detailed error and complexity analysis that allows us to trade efficiency for accuracy.
(iv) We extend the DPS subspace projection to multiple dimensions and describe a novel way to calculate multidimensional DPS sequences using the Kronecker product formalism.

Notation. Let $\mathbb{Z}$, $\mathbb{R}$, and $\mathbb{C}$ denote the set of integers, real and complex numbers, respectively. Vectors are denoted by $\mathbf{v}$ and matrices by $\mathbf{V}$. Their elements are denoted by v_i and $V_{i,l}$, respectively. Transposition of a vector or a matrix is indicated by $\cdot^{\mathrm{T}}$ and conjugate transposition by $\cdot^{\mathrm{H}}$. The Euclidean (ℓ^2) norm of the vector $\mathbf{a}$ is denoted by $\|\mathbf{a}\|$. The Kronecker product and the Khatri-Rao product (columnwise Kronecker product) are denoted by $\otimes$ and $\diamond$, respectively. The inner product of two vectors of length N is defined as $\langle \mathbf{x}, \mathbf{y} \rangle = \sum_{i=0}^{N-1} x_i y_i^*$, where $\cdot^*$ denotes complex conjugation. If X is a discrete index set, $|X|$ denotes the number of elements of X. If X is a continuous region, $|X|$ denotes the Lebesgue measure of X. An N-dimensional sequence $v_{\mathbf{m}}$ is a function from $\mathbf{m} \in \mathbb{Z}^N$ onto $\mathbb{C}$. For an N-dimensional, finite index set $I \subset \mathbb{Z}^N$, the elements of the sequence $v_{\mathbf{m}}$, $\mathbf{m} \in I$, may be collected in a vector $\mathbf{v}$. For a parameterizable function f, $\{f\}$ denotes the family of functions over the whole parameter space. The absolute value, the phase, the real part, and the imaginary part of a complex variable a are denoted by $|a|$, $\Phi(a)$, $\Re a$, and $\Im a$, respectively. $\mathcal{E}\{\cdot\}$ denotes the expectation operator.

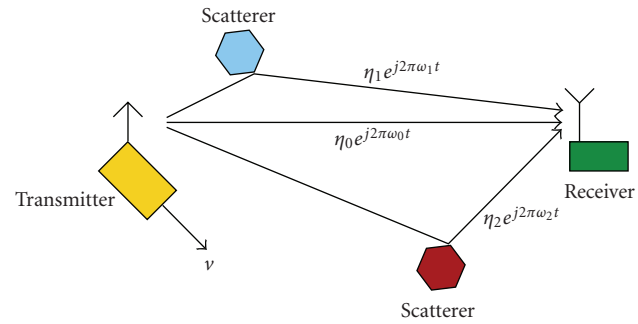

Figure 1: GCM for a time-variant frequency-flat SISO channel. Signals sent from the transmitter, moving at speed v, arrive at the receiver via different paths. Each MPC p has complex weight η_p and Doppler shift ω_p [16].

Organization of the paper

In Section 2, a subspace representation of time-variant frequency-flat SISO channels based on one-dimensional DPS sequences is derived. The main result of the paper, that is, the low-complexity calculation of the basis coefficients of the DPS subspace representation, is given in Section 3. Section 4 extends the DPS subspace representation to higher dimensions, enabling the computer simulation of wideband MIMO channels. A summary and conclusions are given in Section 5. Appendix A proposes a novel way to calculate the multidimensional DPS sequences utilizing the Kronecker product. Appendix B gives a detailed proof of a central theorem. A list of symbols is defined in Appendix C.

2. THE DPS SUBSPACE REPRESENTATION

2.1. Time-variant frequency-flat SISO geometry-based channel model

We start deriving the DPS subspace representation for the generic GCM for time-variant frequency-flat SISO channels depicted in Figure 1. The GCM assumes that the channel transfer function $h(t)$ can be written as a superposition of P MPCs:

$$h(t) = \sum_{p=0}^{P-1} \eta_p e^{2\pi j \omega_p t}, \tag{1}$$

where each MPC is characterized by its complex weight η_p, which embodies the gain and the phase shift, as well as its

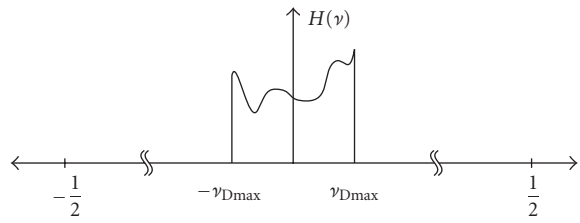

FIGURE 2: Doppler spectrum $H(\nu)$ of the sampled time-variant channel transfer function h_m. The maximum normalized Doppler bandwidth $2\nu_{\mathrm{Dmax}}$ is much smaller than the available normalized channel bandwidth.

Doppler shift ω_p. With $1/T_S$ denoting the sampling rate of the system, the sampled channel transfer function can be written as

$$h_m = h(mT_S) = \sum_{p=0}^{P-1} \eta_p e^{2\pi j \nu_p m}, \tag{2}$$

where $\nu_p = \omega_p T_S$ is the normalized Doppler shift of the pth MPC. We refer to (2) as the sum of complex exponentials (SoCE) algorithm for computing the channel transfer function h_m.

We assume that the normalized Doppler shifts ν_p are bounded by the maximum (one-sided) normalized Doppler bandwidth ν_{Dmax}, which is given by the maximum speed $v_{\max}$ of the transmitter, the carrier frequency f_C, the speed of light c, and the sampling rate $1/T_S$,

$$|\nu_p| \le \nu_{\mathrm{Dmax}} = \frac{v_{\max} f_C}{c} T_S. \tag{3}$$

In typical wireless communication systems, the maximum normalized Doppler bandwidth $2\nu_{\mathrm{Dmax}}$ is much smaller than the available normalized channel bandwidth (see Figure 2):

$$\nu_{\mathrm{Dmax}} \ll \frac{1}{2}. \tag{4}$$

Thus, the channel transfer function (1) is highly oversampled.

Clarke's model [17] is a special case of (2) and assumes that the AoAs ψ_p of the impinging MPCs are distributed uniformly on the interval $[-\pi, \pi)$ and that $\mathcal{E}\{|\eta_p|^2\} = 1/P$. The normalized Doppler shift ν_p of the pth MPC is related to the AoA ψ_p by $\nu_p = \nu_{\mathrm{Dmax}} \cos(\psi_p)$. Jakes' model [8] and its variants [9–14] assume that the AoAs ψ_p are spaced equidistantly with some (random) offset ϑ:

$$\psi_p = \frac{2\pi p + \vartheta}{P}, \quad p = 0, \ldots, P-1. \tag{5}$$

If P is a multiple of four, symmetries can be utilized and only $P/4$ sinusoids have to be evaluated [8]. However, the second-order statistics of such models do not match the ones of Clarke's original model [9].

In this paper, a truncated subspace representation is used to reduce the complexity of the GCM (2). The subspace representation does *not* require special assumptions on the AoAs ψ_p. It is based on DPS sequences, which are introduced in the following section.

2.2. DPS sequences

In this section, one-dimensional DPS sequences are reviewed. They were introduced in 1978 by Slepian [17]. Their applications include spectrum estimation [18], approximation, and prediction of band-limited signals [15, 17] as well as channel estimation in wireless communication systems [6]. DPS sequences can be generalized to multiple dimensions [19]. Multidimensional DPS sequences are reviewed in Section 4.2, where they are used for wideband MIMO channel simulation.

Definition 1. The one-dimensional discrete prolate spheroidal (DPS) sequences $v_m^{(d)}(W, I)$ with band-limit $W = [-\nu_{\mathrm{Dmax}}, \nu_{\mathrm{Dmax}}]$ and concentration region $I = \{M_0, \ldots, M_0 + M - 1\}$ are defined as the real solutions of

$$\sum_{n=M_0}^{M_0+M-1} \frac{\sin\left(2\pi\nu_{\mathrm{Dmax}}(m-n)\right)}{\pi(n-m)} v_n^{(d)}(W, I) = \lambda_d(W, I) v_m^{(d)}(W, I). \tag{6}$$

They are sorted such that their eigenvalues $\lambda_d(W, I)$ are in descending order:

$$\lambda_0(W, I) > \lambda_1(W, I) > \cdots > \lambda_{M-1}(W, I). \tag{7}$$

To ease notation, we drop the explicit dependence of $v_m^{(d)}(W, I)$ on W and I when it is clear from the context. Further, we define the DPS vector $\mathbf{v}^{(d)}(W, I) \in \mathbb{C}^M$ as the DPS sequence $v_m^{(d)}(W, I)$ index-limited to I.

The DPS vectors $\mathbf{v}^{(d)}(W, I)$ are also eigenvectors of the $M \times M$ matrix $\mathbf{K}$ with elements $K_{m,n} = \sin(2\pi\nu_{\mathrm{Dmax}}(m-n))/\pi(n-m)$. The eigenvalues of this matrix decay exponentially and thus render numerical calculation difficult. Fortunately, there exists a tridiagonal matrix commuting with $\mathbf{K}$, which enables fast and numerically stable calculation of DPS sequences [17, 20]. Figures 3 and 4 illustrate one-dimensional DPS sequences and their eigenvalues, respectively.

Some properties of DPS sequences are summarized in the following theorem.

Theorem 1. (1) *The sequences $v_m^{(d)}(W, I)$ are band-limited to W.*

(2) *The eigenvalue $\lambda_d(W, I)$ of the DPS sequence $v_m^{(d)}(W, I)$ denotes the energy concentration of the sequence within I:*

$$\lambda_d(W, I) = \frac{\sum_{m \in I} |v_m^{(d)}(W, I)|^2}{\sum_{m \in \mathbb{Z}} |v_m^{(d)}(W, I)|^2}. \tag{8}$$

(3) *The eigenvalues $\lambda_d(W, I)$ satisfy $1 < \lambda_i(W, I) < 0$. They are clustered around 1 for $d \le D' - 1$, and decay exponentially for $d \ge D'$, where $D' = \lceil |W||I| \rceil + 1$.*

(4) *The DPS sequences $v_m^{(d)}(W, I)$ are orthogonal on the index set I and on $\mathbb{Z}$.*

(5) *Every band-limited sequence h_m can be decomposed uniquely as $h_m = h'_m + g_m$, where h'_m is a linear combination of DPS sequences $v_m^{(d)}(W, I)$ for some I and $g_m = 0$ for all $m \in I$.*

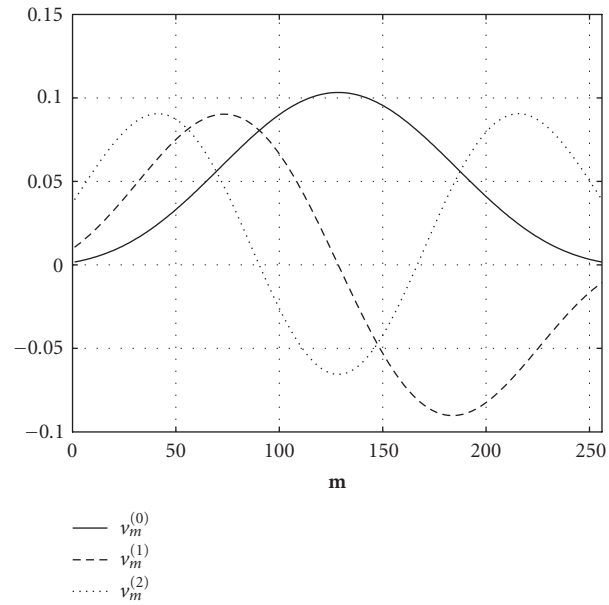

FIGURE 3: The first three one-dimensional DPS sequences $v_m^{(0)}$, $v_m^{(1)}$, and $v_m^{(2)}$ for $M_0 = 0$, $M = 256$, and $M\nu_{\mathrm{Dmax}} = 2$.

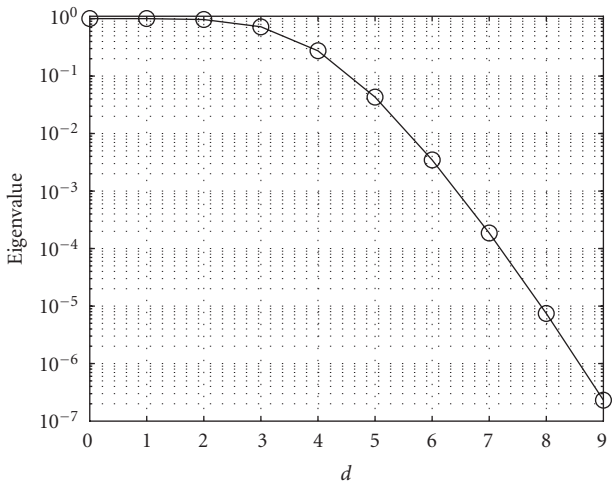

FIGURE 4: The first ten eigenvalues λ_d, $d = 0, \ldots, 9$, of the one-dimensional DPS sequences for $M_0 = 0$, $M = 256$, and $M\nu_{\mathrm{Dmax}} = 2$. The eigenvalues are clustered around 1 for $d \leq D' - 1$, and decay exponentially for $d \geq D'$, where the essential dimension of the signal subspace $D' = \lceil 2\nu_{\mathrm{Dmax}} M \rceil + 1 = 5$.

Proof. See Slepian [17]. □

2.3. DPS subspace representation

The time-variant fading process $\{h_m\}$ given by the model in (2) is band-limited to the region $W = [-\nu_{\mathrm{Dmax}}, \nu_{\mathrm{Dmax}}]$. Let $I = \{M_0, \ldots, M_0 + M - 1\}$ denote a finite index set on which we want to calculate h_m. Due to property (5) of Theorem 1, h_m can be decomposed into $h_m = h'_m + g_m$, where h'_m is a linear combination of the DPS sequences $v_m^{(d)}(W, I)$ and $h_m = h'_m$ for all $m \in I$. Therefore, the vectors

$$\mathbf{h} = \left[h_{M_0}, h_{M_0+1}, \ldots, h_{M_0+M-1}\right]^T \in \mathbb{C}^M \tag{9}$$

obtained by index limiting h_m to I can be represented as a linear combination of the DPS vectors

$$\mathbf{v}^{(d)}(W, I) = \left[v_{M_0}^{(d)}(W, I), v_{M_0+1}^{(d)}(W, I), \ldots, v_{M_0+M-1}^{(d)}(W, I)\right]^T \in \mathbb{C}^M. \tag{10}$$

Properties (2) and (3) of Theorem 1 show that the first $D' = \lceil 2\nu_{\mathrm{Dmax}} M \rceil + 1$ DPS sequences contain almost all of their energy in the index-set I. Therefore, the vectors $\{\mathbf{h}\}$ span a subspace with essential dimension [6]

$$D' = \lceil 2M\nu_{\mathrm{Dmax}} \rceil + 1. \tag{11}$$

Due to (4), the time-variant fading process is highly oversampled. Thus the maximum number of subspace dimensions M is reduced by $2\nu_{\mathrm{Dmax}} \ll 1$. In typical wireless communication systems, the essential subspace dimension D' is in the order of two to five only. This fact is exploited in the following definition.

Definition 2. Let $\mathbf{h}$ be a vector obtained by index limiting a band-limited process with band-limit W to the index set I. Further, collect the first D DPS vectors $\mathbf{v}^{(d)}(W, I)$ in the matrix

$$\mathbf{V} = \left[\mathbf{v}^{(0)}(W, I), \ldots, \mathbf{v}^{(D-1)}(W, I)\right]. \tag{12}$$

The *DPS subspace representation* of $\mathbf{h}$ with dimension D is defined as

$$\hat{\mathbf{h}}^D = \mathbf{V}\boldsymbol{\alpha}, \tag{13}$$

where $\boldsymbol{\alpha}$ is the projection of the vector $\mathbf{h}$ onto the columns of $\mathbf{V}$:

$$\boldsymbol{\alpha} = \mathbf{V}^H \mathbf{h}. \tag{14}$$

For the purpose of channel simulation, it is possible to use $D > D'$ DPS vectors in order to increase the numerical accuracy of the subspace representation. The subspace dimension D has to be chosen such that the bias of the subspace representation is small compared to the machine precision of the underlying simulation hardware. This is illustrated in Section 3.2 by numerical examples.

In terms of complexity, the problem of computing the series (2) was reformulated into the problem of computing the basis coefficients $\boldsymbol{\alpha}$ of the subspace representation (13). If they were computed directly using (14), the complexity of the problem would not be reduced. In the following section, we derive a novel low-complexity method to calculate the basis coefficients $\boldsymbol{\alpha}$ approximately.

3. MAIN RESULT

3.1. Approximate calculation of the basis coefficients

In this section, an approximate method to calculate the basis coefficients $\boldsymbol{\alpha}$ in (13) with low complexity is presented. Until now we have only considered the time domain of the channel and assumed that the band limiting region W is symmetric around the origin. To make the methods in this section also applicable to the frequency domain and the spatial domains (cf. Section 4), we make the more general assumption that

$$W = [W_0 - W_{\max}, W_0 + W_{\max}]. \tag{15}$$

The projection of a single complex exponential vector $\mathbf{e}_p = [e^{2\pi j\nu_p M_0}, \ldots, e^{2\pi j\nu_p (M_0+M-1)}]^T$ onto the basis functions $\mathbf{v}^{(d)}(W,I)$ can be written as a function of the Doppler shift ν_p, the band-limit region W, and the index set I,

$$\gamma_d(\nu_p; W, I) = \sum_{m=M_0}^{M_0+M-1} v_m^{(d)}(W,I) e^{2\pi j m\nu_p}. \tag{16}$$

Since $\mathbf{h}$ can be written as

$$\mathbf{h} = \sum_{p=0}^{P-1} \eta_p \mathbf{e}_p, \tag{17}$$

the basis coefficients $\boldsymbol{\alpha}$ (14) can be calculated by

$$\boldsymbol{\alpha} = \sum_{p=0}^{P-1} \eta_p \mathbf{V}^H \mathbf{e}_p = \sum_{p=0}^{P-1} \eta_p \boldsymbol{\gamma}_p, \tag{18}$$

where $\boldsymbol{\gamma}_p = [\gamma_0(\nu_p; W, I), \ldots, \gamma_{D-1}(\nu_p; W, I)]^T$ denote the basis coefficients for a single MPC.

To calculate the basis coefficients $\gamma_d(\nu_p; W, I)$, we take advantage of the DPS wave functions $U_d(f; W, I)$. For the special case $W_0 = 0$ and $M_0 = 0$ the DPS wave functions are defined in [17]. For the more general case, the DPS wave functions are defined as the eigenfunctions of

$$\begin{aligned} &\int_W \frac{\sin(M\pi(\nu-\nu'))}{\sin(\pi(\nu-\nu'))} U_d(\nu'; W, I) d\nu \\ &\quad = \lambda_d(W,I) U_d(\nu; W, I), \quad \nu \in W. \end{aligned} \tag{19}$$

They are normalized such that

$$\begin{aligned} &\int_W |U_d(\nu; W, I)|^2 d\nu = 1, \\ &U_d(W_0; W, I) \geq 0, \qquad \left.\frac{dU_d(\nu; W, I)}{df}\right|_{\nu=W_0} \geq 0, \\ &\qquad\qquad d = 0, \ldots, D-1. \end{aligned} \tag{20}$$

The DPS wave functions are closely related to the DPS sequences. It can be shown that the amplitude spectrum of a DPS sequence limited to $m \in I$ is a scaled version of the associated DPS wave function (cf. [17, equation (26)])

$$U_d(\nu; W, I) = \epsilon_d \sum_{m=M_0}^{M_0+M-1} v_m^{(d)}(W,I) e^{-j\pi(2M_0+M-1-2m)\nu}, \tag{21}$$

where $\epsilon_d = 1$ if d is even, and $\epsilon_d = j$ if d is odd.

Comparing (16) with (21) shows that the basis coefficients can be calculated according to

$$\gamma_d(\nu_p; W, I) = \frac{1}{\epsilon_d} e^{j\pi(2M_0+M-1)\nu_p} U_d(\nu_p; W, I). \tag{22}$$

The following definition and theorem show that $U_d(\nu_p; W, I)$ can be approximately calculated from $v_m^{(d)}(W,I)$ by a simple scaling and shifting operation [21].

Definition 3. Let $v_m^{(d)}(W,I)$ be the DPS sequences with band-limit region $W = [W_0 - W_{\max}, W_0 + W_{\max}]$ and index set $I = \{M_0, \ldots, M_0 + M - 1\}$. Further denote by $\lambda_d(W,I)$ the corresponding eigenvalues. For $\nu_p \in W$ define the index m_p by

$$m_p = \left\lfloor \left(1 + \frac{\nu_p - W_0}{W_{\max}}\right) \frac{M}{2} \right\rfloor. \tag{23}$$

Approximate DPS wave functions are defined as

$$\widetilde{U}_d(\nu_p; W, I) := \pm e^{2\pi j(M_0+M-1+m_p)W_0} \sqrt{\frac{\lambda_d M}{2W_{\max}}} v_{m_p}^{(d)}(W,I), \tag{24}$$

where the sign is taken such that the following normalization holds:

$$\begin{aligned} &\widetilde{U}_d(W_0; W, I) \geq 0, \qquad \left.\frac{d\widetilde{U}_d(\nu_p; W, I)}{d\nu_p}\right|_{\nu_p=W_0} \geq 0, \\ &\qquad\qquad d = 0, \ldots, D-1. \end{aligned} \tag{25}$$

Theorem 2. *Let $\psi_d(c, f)$ be the prolate spheroidal wave functions [22]. Let $c > 0$ be given and set*

$$M = \left\lfloor \frac{c}{\pi W_{\max}} \right\rfloor. \tag{26}$$

If $W_{\max} \to 0$,

$$\begin{aligned} \sqrt{W_{\max}}\, \widetilde{U}_d(W_{\max}\nu_p; W, I) &\sim \psi_d(c, \nu_p), \\ \sqrt{W_{\max}}\, U_d(W_{\max}\nu_p; W, I) &\sim \psi_d(c, \nu_p). \end{aligned} \tag{27}$$

In other words, both the approximate DPS wave functions as well as the DPS wave functions themselves converge to the prolate spheroidal wave functions.

Proof. For $W_0 = 0$ and $M_0 = 0$, that is, $W' = [-W_{\max}, W_{\max}]$ and $I' = \{0, \ldots, M-1\}$ the proof is given in [17, Section 2.6]. The general case follows by using the two identities

$$\begin{aligned} v_m^{(d)}(W,I) &= e^{2\pi j(m+M_0)W_0} v_{m+M_0}^{(d)}(W', I'), \\ U_d(\nu, W, I) &= e^{\pi j(2M_0+M-1)(\nu-W_0)} U_d(\nu - W_0; W', I'). \end{aligned} \tag{28}$$

□

Theorem 2 suggests that the approximate DPS wave functions can be used as an approximation to the DPS wave functions. Therefore, the basis coefficients (22) can be calculated approximately by

$$\widetilde{\gamma}_d(\nu_p; W, I) := \frac{1}{\epsilon_d} e^{j\pi(2M_0+M-1)\nu_p} \widetilde{U}_d(\nu_p; W, I). \tag{29}$$

The theorem does not indicate the quality of the approximation. It can only be deduced that the approximation improves as the bandwidth $W_{\max}$ decreases, while the number of samples $M = \lfloor c/\pi W_{\max} \rfloor$ increases. This fact is exploited in the following definition.

Definition 4. Let $\mathbf{h}$ be a vector obtained by index limiting a band-limited process of the form (2) with band-limit $W = [W_0 - W_{\max}, W_0 + W_{\max}]$ to the index set $I = \{M_0, \ldots, M_0 + M - 1\}$. For a positive integer r—*the resolution factor*—define

$$\begin{aligned} I_r &= \{M_0, M_0 + 1, \ldots, M_0 + rM - 1\}, \\ W_r &= \left[W_0 - \frac{W_{\max}}{r}, W_0 + \frac{W_{\max}}{r} \right]. \end{aligned} \tag{30}$$

The *approximate DPS subspace representation* with dimension D and resolution factor r is given by

$$\widetilde{\mathbf{h}}^{D,r} = \mathbf{V}\widetilde{\boldsymbol{\alpha}}^r \tag{31}$$

whose *approximate basis coefficients* are

$$\widetilde{\alpha}_d^r = \sum_{p=0}^{P-1} \eta_p \widetilde{\gamma}_d\left(\frac{\nu_p}{r}, W_r, I_r\right). \tag{32}$$

Note that the DPS sequences are required in a higher resolution only for the calculation of the approximate basis coefficients. The resulting $\widetilde{\mathbf{h}}^{D,r}$ has the same sample rate for any choice of r.

3.2. Bias of the subspace representation

In this subsection, the square bias of the subspace representation

$$\text{bias}^2_{\widehat{\mathbf{h}}^D} = \mathcal{E}\left\{ \frac{1}{M} ||\mathbf{h} - \widehat{\mathbf{h}}^D||^2 \right\} \tag{33}$$

and the square bias of the approximate subspace representation

$$\text{bias}^2_{\widetilde{\mathbf{h}}^{D,r}} = \mathcal{E}\left\{ \frac{1}{M} ||\mathbf{h} - \widetilde{\mathbf{h}}^{D,r}||^2 \right\} \tag{34}$$

are analyzed.

For ease of notation, we assume again that $W = [-\nu_{\text{Dmax}}, \nu_{\text{Dmax}}]$, that is, we set $W_0 = 0$ and $W_{\max} = \nu_{\text{Dmax}}$. However, the results also hold for the general case (15). If the Doppler shifts ν_p, $p = 0, \ldots, P-1$, are distributed independently and uniformly on W, the DPS subspace representation $\widehat{\mathbf{h}}$ coincides with the Karhunen-Loève transform of $\mathbf{h}$ [23] and it can be shown that

$$\text{bias}^2_{\widehat{\mathbf{h}}^D} = \frac{1}{M\nu_{\text{Dmax}}} \sum_{d=D}^{M-1} \lambda_d(W, I). \tag{35}$$

Table 1: Simulation parameters for the numerical experiments in the time domain. The carrier frequency and the sample rate resemble those of a UMTS system [24]. The block length is chosen to be as long as a UMTS frame.

Parameter	Value
Carrier frequency f_c	2 GHz
Sample rate $1/T_S$	3.84 MHz
Block length M	2560 samples
Mobile velocity $v_{\max}$	100 km/h
Maximum norm. Doppler ν_{Dmax}	4.82×10^{-5}

If the Doppler shifts ν_p, $p = 0, \ldots, P-1$, are not distributed uniformly, (35) can still be used as an approximation for the square bias [21].

For the square bias of the approximate DPS subspace representation $\widetilde{\mathbf{h}}^{D,r}$, no analytical results are available. However, for the minimum achievable square bias, we conjecture that

$$\text{bias}^2_{\min,r} = \min_D \text{bias}^2_{\widetilde{\mathbf{h}}^{D,r}} \approx \left(\frac{2\nu_{\text{Dmax}}}{r} \right)^2. \tag{36}$$

This conjecture is substantiated by numerical Monte-Carlo simulations using the parameters from Table 1. The Doppler shifts ν_p, $p = 0, \ldots, P-1$, are distributed independently and uniformly on W. The results are illustrated in Figure 5. It can be seen that the square bias of the subspace representation $\text{bias}^2_{\widehat{\mathbf{h}}^D}$ decays with the subspace dimension. For $D \geq \lceil 2M\nu_{\text{Dmax}} \rceil + 1 = 2$ this decay is even exponential. These two properties can also be seen directly from (35) and the exponential decay of the eigenvalues $\lambda_d(W, I)$. The square bias $\text{bias}^2_{\widetilde{\mathbf{h}}^{D,r}}$ of the approximate subspace representation is similar to $\text{bias}^2_{\widehat{\mathbf{h}}^D}$ up to a certain subspace dimension. Thereafter, the square bias of the approximate subspace representation levels out at $\text{bias}^2_{\min,r} \approx (2\nu_{\text{Dmax}}/r)^2$. Increasing the resolution factor pushes the levels further down.

Let the maximal allowable square error of the simulation be denoted by $E^2_{\max}$. Then, the approximate subspace representation can be used without loss of accuracy if D and r are chosen such that

$$\text{bias}^2_{\widetilde{\mathbf{h}}^{D,r}} \overset{!}{\leq} E^2_{\max}. \tag{37}$$

Good approximations for D and r can be found by

$$D = \operatorname*{argmin}_D \text{bias}^2_{\widehat{\mathbf{h}}^D} \leq E^2_{\max}, \qquad r = \operatorname*{argmin}_r \text{bias}^2_{\min,r} \leq E^2_{\max}. \tag{38}$$

The first expression can be computed using (35). Using conjecture (36), the latter evaluates to

$$r = \left\lfloor \frac{2\nu_{\text{Dmax}}}{E_{\max}} \right\rfloor. \tag{39}$$

Using a 14-bit fixed-point processor, the maximum achievable accuracy is $E^2_{\max} = (2^{-13})^2 \approx 1.5 \times 10^{-8}$. For the example of Figure 5, where the maximum Doppler shift $\nu_{\text{Dmax}} = 4.82 \times 10^{-5}$ and the number of samples $M = 2560$, the choice $D = 4$ and $r = 2$ makes the simulation as accurate as possible on this hardware. Depending on the application, a lower accuracy might also be sufficient.

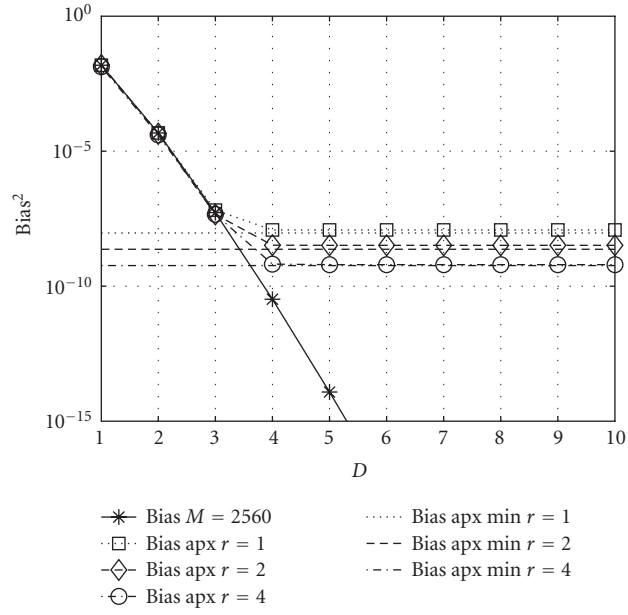

FIGURE 5: $\text{bias}^2_{\tilde{\mathbf{h}}_D}$ (denoted by "bias"), $\text{bias}^2_{\tilde{\mathbf{h}}_{D,r}}$ (denoted by "bias apx"), and $\text{bias}^2_{\min,r}$ (denoted by "bias apx min") for $\nu_{\text{Dmax}} = 4.82 \times 10^{-5}$ and $M = 2560$. The factor r denotes the resolution factor.

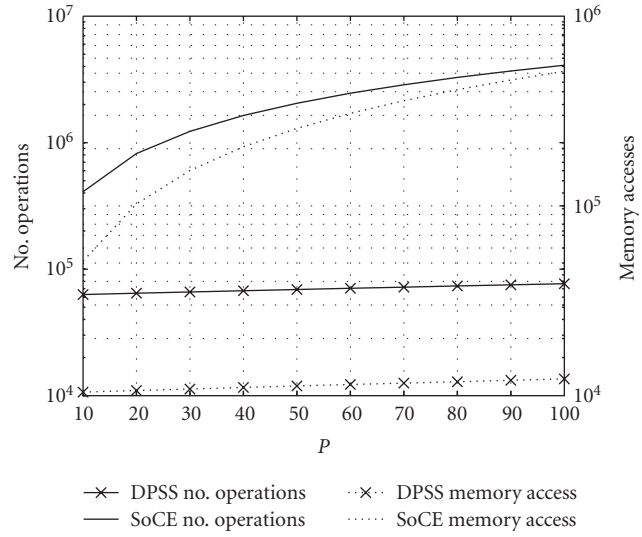

FIGURE 6: Complexity in terms of number of arithmetic operations (left abscissa) and memory access operations (right abscissa) versus the number of MPCs P. We show results for the sum of complex exponentials algorithm (denoted by "SoCE") and the approximate subspace representation (denoted by "DPSS") using $M = 2560$, $\nu_{\text{Dmax}} = 4.82 \times 10^{-5}$, and $D = 4$.

3.3. Complexity and memory requirements

In this subsection, the computational complexity of the approximate subspace representation (31) is compared to the SoCE algorithm (2). The complexity is expressed in number of complex multiplications (CM) and evaluations of the complex exponential (CE). Additionally, we compare the number of memory access (MA) operations, which gives a better complexity comparison than the actual memory requirements.

We assume that all complex numbers are represented using their real and imaginary part. A CM thus requires four multiplication and two addition operations. As a reference for a CE we use a table look-up implementation with linear interpolation for values between table elements [2]. This implementation needs six addition, four multiplication, and two memory access operations.

Let the number of operations that are needed to evaluate $\mathbf{h}$ and $\tilde{\mathbf{h}}$ be denoted by $C_{\mathbf{h}}$ and $C_{\tilde{\mathbf{h}}}$, respectively. Using the SoCE algorithm, for every $m \in I = \{M_0, \ldots, M_0+M-1\}$ and every $p = 0, \ldots, P-1$, a CE and a CM have to be evaluated, that is,

$$C_{\mathbf{h}} = MP\ \text{CE} + MP\ \text{CM}. \tag{40}$$

For the approximate DPS subspace representation with dimension D, first the approximate basis coefficients $\tilde{\boldsymbol{\alpha}}$ have to be evaluated, requiring

$$C_{\tilde{\boldsymbol{\alpha}}} = DP(\text{CE} + 2\ \text{CM} + \ \text{MA}) + DP\ \text{CM} \tag{41}$$

operations where the first term accounts for (29) and the second term for (32). In total, for the evaluation of the approximate subspace representation (31),

$$C_{\tilde{\mathbf{h}}} = MD(\text{CM} + \text{MA}) + C_{\tilde{\boldsymbol{\alpha}}} \tag{42}$$

operations are required. For large P, the approximate DPS subspace representation reduces the number of arithmetic operations compared to the SoCE algorithm by

$$\frac{C_{\mathbf{h}}}{C_{\tilde{\mathbf{h}}}} \longrightarrow \frac{M(\text{CE} + \text{CM})}{D(\text{CE} + 3\ \text{CM})}. \tag{43}$$

The memory requirements of the DPS subspace representation are determined by the block length M, the subspace dimension D and the resolution factor r. If the DPS sequences are stored with 16-bit precision,

$$\text{Mem}_{\tilde{\mathbf{h}}} = 2rMD\ \text{byte} \tag{44}$$

are needed.

In Figure 6, $C_{\mathbf{h}}$ and $C_{\tilde{\mathbf{h}}}$ are plotted over the number of paths P for the parameters given in Table 1. Multiplications and additions are counted as one operation. Memory access operations are counted separately. The subspace dimension is chosen to be $D = 4$ according to the observations of the last subsection. The memory requirements for the DPS subspace representation are $\text{Mem}_{\tilde{\mathbf{h}}} = 80$ kbyte.

It can be seen that the complexity of the approximate DPS subspace representation in terms of number of arithmetic operations as well as memory access operations increases with slope D, while the complexity of the SoCE algorithm increases with slope M. Since in the given example

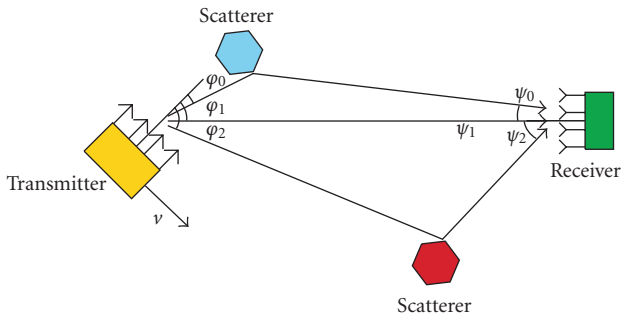

FIGURE 7: Multipath propagation model for a time-variant wideband MIMO radio channel. The signals sent from the transmitter, moving at speed v, arrive at the receiver. Each path p has complex weight η_p, time delay τ_p, Doppler shift ω_p, angle of departure φ_p, and angle of arrival ψ_p.

$D \ll M$, the approximate DPS subspace representation already enables a complexity reduction by more than one order of magnitude compared to the SoCE algorithm for $P = 30$ paths. Asymptotically, the number of arithmetic operations can be reduced by a factor of $C_{\mathbf{h}}/C_{\tilde{\mathbf{h}}} \to 465$.

4. WIDEBAND MIMO CHANNEL SIMULATION

4.1. The wideband MIMO geometry-based channel model

The time-variant GCM described in Section 2.1 can be extended to describe time-variant wideband MIMO channels. For simplicity we assume uniform linear arrays (ULA) with omnidirectional antennas. Then the channel can be described by the time-variant wideband MIMO channel transfer function $h(t, f, x, y)$, where t denotes time, f denotes frequency, x the position of the transmit antenna on the ULA, y the position of the receive antenna on the ULA [25].

The GCM assumes that $h(t, f, x, y)$ can be written as a superposition of P MPCs,

$$h(t,f,x,y) = \sum_{p=0}^{P-1} \eta_p e^{2\pi j \omega_p t} e^{-2\pi j \tau_p f} e^{2\pi j/\lambda \sin\varphi_p x} e^{-2\pi j/\lambda \sin\psi_p y}, \tag{45}$$

where every MPC is characterized by its complex weight η_p, its Doppler shift ω_p, its delay τ_p, its angle of departure (AoD) φ_p, and its AoA ψ_p (see Figure 7) and λ is the wavelength. More sophisticated models may also include parameters such as elevation angle, antenna patterns, and polarization.

There exist many models for how to obtain the parameters of the MPCs. They can be categorized as *deterministic*, *geometry-based stochastic*, and *nongeometrical stochastic* models [26]. The number of MPCs required depends on the scenario modeled, the system bandwidth, and the number of antennas used. In this paper, we choose the number of MPCs such that the channel is Rayleigh fading, except for the line-of-sight component.

For narrowband frequency-flat systems, approximately $P_0 = 40$ MPCs are needed to achieve a Rayleigh fading statistics [13]. If the channel bandwidth is increased, the number of resolvable MPCs increases also. The ITU channel models [27], which are used for bandwidths up to 5 MHz in UMTS systems, specify a power delay profile with up to six delay bins. The I-METRA channel models for the IEEE 802.11n wireless LAN standard [28] are valid for up to 40 MHz and specify a power delay profile with up to 18 delay bins. This requires a total number of MPCs of up to $P_1 = 18P_0 = 720$. Diffuse scattering can also be modeled using a GCM by increasing the number of MPCs. In theory, diffuse scattering results from the superposition of an infinite number of MPCs [29]. However, good approximations can be achieved by using a large but finite number of MPCs [30, 31]. In MIMO channels, the number of MPCs multiplies by $N_{\mathrm{Tx}}N_{\mathrm{Rx}}$, since every antenna sees every scatterer from a different AoA and AoD, respectively. For a 4×4 system, the total number of MPCs can thus reach up to $P = 16P_1 = 1.2 \times 10^4$.

We now show that the sampled time-variant wideband MIMO channel transfer function is band-limited in time, frequency, and space. Let F_S denote the width of a frequency bin and D_S the distance between antennas. The sampled channel transfer function can be described as a four-dimensional sequence $h_{m,q,r,s} = h(mT_S, qF_S, rD_S, sD_S)$, where m denotes discrete time, q denotes discrete frequency, s denotes the index of the transmit antenna, and r denotes the index of the receive antenna.[1] Further, let $\nu_p = \omega_p T_S$ denote the normalized Doppler shift, $\theta_p = \tau_p F_S$ the normalized delay, $\zeta_p = \sin(\varphi_p)D_S/\lambda$ and $\xi_p = \sin(\psi_p)D_S/\lambda$ the normalized angles of departure and arrival, respectively. If all these indices are collected in the vectors

$$\begin{aligned} \mathbf{m} &= [m, q, s, r]^T, \\ \mathbf{f}_p &= [\nu_p, -\theta_p, \zeta_p, -\xi_p]^T, \end{aligned} \tag{46}$$

$h_{\mathbf{m}}$ can be written as

$$h_{\mathbf{m}} = \sum_{p=0}^{P-1} \eta_p e^{j2\pi\langle \mathbf{f}_p, \mathbf{m}\rangle}, \tag{47}$$

that is, the multidimensional form of (2).

The band-limitation of $h_{\mathbf{m}}$ in time, frequency, and space is defined by the following physical parameters of the channel.

(1) The maximum normalized Doppler shift of the channel ν_{Dmax} defines the band-limitation in the time domain. It is determined by the maximum speed of the user $v_{\max}$, the carrier frequency f_C, the speed of light c, and the sampling rate $1/T_S$, that is,

$$\nu_{\mathrm{Dmax}} = \frac{v_{\max} f_C}{c} T_S. \tag{48}$$

[1] In the literature, the time-variant wideband MIMO channel is often represented by the matrix $\mathbf{H}(m, q)$, whose elements are related to the sampled time-variant wideband MIMO channel transfer function $h_{m,q,r,s}$ by $H_{r,s}(m, q) = h_{m,q,r,s}$.

(2) The maximum normalized delay of the scenario $\theta_{\max}$ defines the band-limitation in the frequency domain. It is determined by the maximum delay $\tau_{\max}$ and the sample rate $1/F_S$ in frequency

$$\theta_{\max} = \tau_{\max} F_S. \tag{49}$$

(3) The minimum and maximum normalized AoA, $\xi_{\min}$ and $\xi_{\max}$ define the band-limitation in the spatial domain at the receiver. They are given by the minimum and maximum AoA, $\psi_{\min}$ and $\psi_{\max}$, the spatial sampling distance D_S and the wavelength λ:

$$\xi_{\min} = \sin(\psi_{\min})\frac{D_S}{\lambda}, \qquad \xi_{\max} = \sin(\psi_{\max})\frac{D_S}{\lambda}. \tag{50}$$

The band-limitation at the transmitter is given similarly by the normalized minimum and maximum normalized AoD, $\zeta_{\min}$ and $\zeta_{\max}$.

In summary it can be seen that $h_{\mathbf{m}}$ is band-limited to

$$W = [-\nu_{\mathrm{Dmax}}, \nu_{\mathrm{Dmax}}] \times [0, \theta_{\max}] \times [\zeta_{\min}, \zeta_{\max}] \times [\xi_{\min}, \xi_{\max}]. \tag{51}$$

Thus the discrete time Fourier transform (DTFT)

$$H(\mathbf{f}) = \sum_{\mathbf{m}\in\mathbb{Z}^N} h_{\mathbf{m}} e^{-2\pi j\langle \mathbf{f},\mathbf{m}\rangle}, \quad \mathbf{f}\in\mathbb{C}^N, \tag{52}$$

vanishes outside the region W, that is,

$$H(\mathbf{f}) = 0, \quad \mathbf{f}\notin W. \tag{53}$$

4.2. Multidimensional DPS sequences

The fact that $h_{\mathbf{m}}$ is band-limited allows one to extend the concepts of the DPS subspace representation also to time-variant wideband MIMO channels. Therefore, a generalization of the one-dimensional DPS sequences to multiple dimensions is required.

Definition 5. Let $I \subset \mathbb{Z}^N$ be an N-dimensional finite index set with $L = |I|$ elements, and $W \subset (-1/2, 1/2)^N$ an N-dimensional band-limiting region. *Multidimensional discrete prolate spheroidal (DPS) sequences* $v_{\mathbf{m}}^{(d)}(W,I)$ are defined as the solutions of the eigenvalue problem

$$\sum_{\mathbf{m}'\in I} v_{\mathbf{m}'}^{(d)}(W,I) K^{(W)}(\mathbf{m}'-\mathbf{m}) = \lambda_d(W,I) v_{\mathbf{m}}^{(d)}(W,I), \quad \mathbf{m}\in\mathbb{Z}^N, \tag{54}$$

where

$$K^{(W)}(\mathbf{m}'-\mathbf{m}) = \int_W e^{2\pi j\langle \mathbf{f}'',\mathbf{m}'-\mathbf{m}\rangle} d\mathbf{f}''. \tag{55}$$

They are sorted such that their eigenvalues $\lambda_d(W,I)$ are in descending order

$$\lambda_0(W,I) > \lambda_1(W,I) > \cdots > \lambda_{L-1}(W,I). \tag{56}$$

To ease notation, we drop the explicit dependence of $v_{\mathbf{m}}^{(d)}(W,I)$ on W and I when it is clear from the context. Further, we define the multidimensional DPS vector $\mathbf{v}^{(d)}(W,I) \in \mathbb{C}^L$ as the multidimensional DPS sequence $v_{\mathbf{m}}^{(d)}(W,I)$ index-limited to I. In particular, if every element $\mathbf{m}\in I$ is indexed lexicographically, such that $I = \{\mathbf{m}_l, l = 0,1,\ldots,L-1\}$, then

$$\mathbf{v}^{(d)}(W,I) = \left[v_{\mathbf{m}_0}^{(d)}(W,I),\ldots,v_{\mathbf{m}_{L-1}}^{(d)}(W,I)\right]^T. \tag{57}$$

All the properties of Theorem 1 also apply to multidimensional DPS sequences [19]. The only difference is that m has to be replaced with $\mathbf{m}$ and $\mathbb{Z}$ with $\mathbb{Z}^N$.

Example 1. In the two-dimensional case $N = 2$ with band-limiting region W and index set I given by

$$W = [-\nu_{\mathrm{Dmax}}, \nu_{\mathrm{Dmax}}] \times [0, \theta_{\max}],$$
$$I = \{0,\ldots,M-1\} \times \left\{-\left\lfloor\frac{Q}{2}\right\rfloor,\ldots,\left\lfloor\frac{Q}{2}\right\rfloor - 1\right\}. \tag{58}$$

Equation (54) reduces to

$$\sum_{n=0}^{M-1}\sum_{p=-\lfloor Q/2\rfloor}^{\lfloor Q/2\rfloor-1} \frac{\sin(2\pi\nu_{\mathrm{Dmax}}(m-n))}{\pi(n-m)} \frac{e^{2\pi i(p-q)\theta_{\max}}-1}{2\pi i(p-q)} v_{n,p}^{(d)} = \lambda_d v_{m,q}^{(d)}. \tag{59}$$

Note that due to the nonsymmetric band-limiting region W, the solutions of (59) can take complex values. Examples of two-dimensional DPS sequences and their eigenvalues are given in Figures 8 and 9, respectively. They have been calculated using the methods described in Appendix A.

4.3. Multidimensional DPS subspace representation

We assume that for hardware implementation, $h_{\mathbf{m}}$ is calculated blockwise for M samples in time, Q bins in frequency, N_{Tx} transmit antennas, and N_{Rx} receive antennas. Accordingly, the index set is defined by

$$I = \{0,\ldots,M-1\} \times \left\{-\left\lfloor\frac{Q}{2}\right\rfloor,\ldots,\left\lfloor\frac{Q}{2}\right\rfloor - 1\right\} \times \{0,\ldots,N_{\mathrm{Tx}}-1\} \times \{0,\ldots,N_{\mathrm{Rx}}-1\}. \tag{60}$$

The DPS subspace representation can easily be extended to multiple dimensions. Let $\mathbf{h}$ be the vector obtained by index limiting the sequence $h_{\mathbf{m}}$ (47) to the index set I (60) and sorting the elements lexicographically. In analogy to the one-dimensional case, the subspace spanned by $\{\mathbf{h}\}$ is also spanned by the multidimensional DPS vectors $\mathbf{v}^{(d)}(W,I)$ defined in Section 4.2. Due to the common notation of one- and multidimensional sequences and vectors, the *multidimensional DPS subspace representation* of $\mathbf{h}$ can be defined similarly to Definition 2.

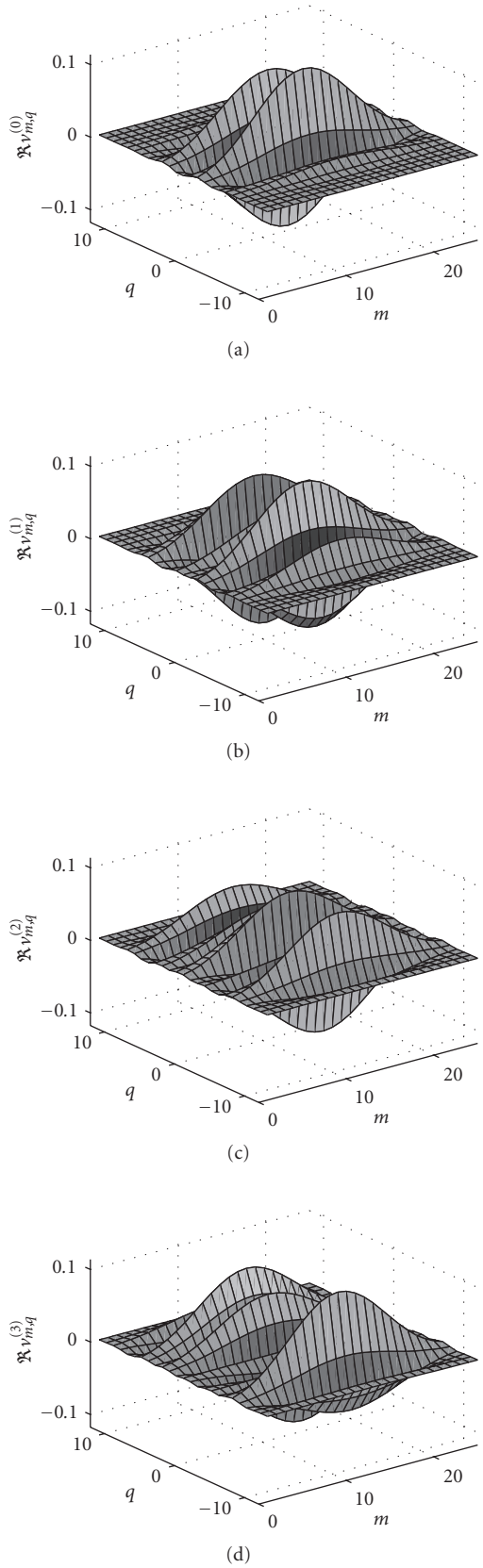

FIGURE 8: The real part of the first four two-dimensional DPS sequences $v^{(d)}_{m,q}$, $d = 0,\ldots,3$ for $M = Q = 25$, $M\nu_{\mathrm{Dmax}} = 2$, and $Q\theta_{\max} = 5$.

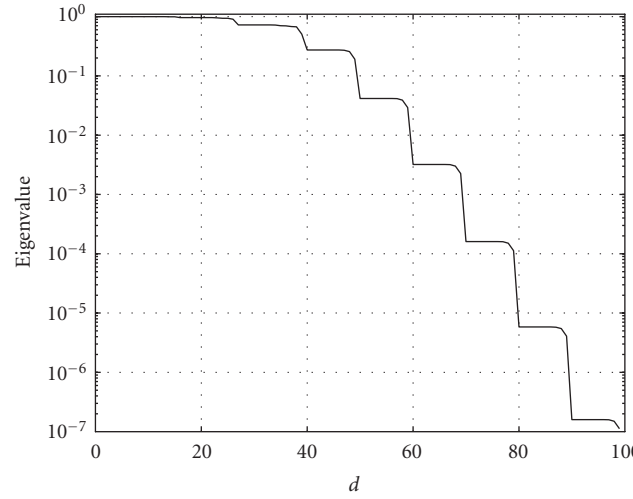

FIGURE 9: First 100 eigenvalues λ_d, $d = 0,\ldots,99$, of two-dimensional DPS sequences for $M = Q = 25$, $M\nu_{\mathrm{Dmax}} = 2$, and $Q\theta_{\max} = 5$. The eigenvalues are clustered around 1 for $d \le D' - 1$, and decay exponentially for $d \ge D'$, where the essential dimension of the signal subspace $D' = \lceil |W||I| \rceil + 1 = 41$.

Definition 6. Let $\mathbf{h}$ be a vector obtained by index limiting a multidimensional band-limited process of the form (47) with band-limit W to the index set I. Let $\mathbf{v}^{(d)}(W,I)$ be the multidimensional DPS vectors for the multidimensional band-limit region W and the multidimensional index set I. Further, collect the first D DPS vectors $\mathbf{v}^{(d)}(W,I)$ in the matrix

$$\mathbf{V} = \left[\mathbf{v}^{(0)}(W,I),\ldots,\mathbf{v}^{(D-1)}(W,I)\right]. \tag{61}$$

The *multidimensional DPS subspace representation* of $\mathbf{h}$ with subspace dimension D is defined as

$$\widehat{\mathbf{h}}^D = \mathbf{V}\boldsymbol{\alpha}, \tag{62}$$

where $\boldsymbol{\alpha}$ is the projection of the vector $\mathbf{h}$ onto the columns of $\mathbf{V}$:

$$\boldsymbol{\alpha} = \mathbf{V}^H\mathbf{h}. \tag{63}$$

The subspace dimension D has to be chosen such that the bias of the subspace representation is small compared to the machine precision of the underlying simulation hardware. The following theorem shows how the multidimensional projection (63) can be reduced to a series of one-dimensional projections.

Theorem 3. *Let $\widehat{\mathbf{h}}^D$ be the N-dimensional DPS subspace representation of $\mathbf{h}$ with subspace dimension D, band-limiting region W, and index set I. If W and I can be written as Cartesian products*

$$W = W_0 \times \cdots \times W_{N-1}, \tag{64}$$

$$I = I_0 \times \cdots \times I_{N-1}, \tag{65}$$

where $W_i = [W_{0,i} - W_{\max,i}, W_{0,i} + W_{\max,i}]$, *and* $I_i = \{M_{0,i}, \ldots, M_{0,i} + M_i - 1\}$, *then for every* $d = 0, \ldots, D-1$, *there exist* $d_0, \ldots, d_{N-1}$ *such that the* N*-dimensional DPS basis vectors* $\mathbf{v}^{(d)}(W, I)$ *can be written as*

$$\mathbf{v}^{(d)}(W, I) = \mathbf{v}^{(d_0)}(W_0, I_0) \otimes \cdots \otimes \mathbf{v}^{(d_{N-1})}(W_{N-1}, I_{N-1}). \tag{66}$$

Further, the basis coefficients of the approximate DPS subspace representation

$$\widetilde{\mathbf{h}}^D = \mathbf{V}\widetilde{\boldsymbol{\alpha}} \tag{67}$$

are given by

$$\widetilde{\boldsymbol{\alpha}} = \sum_{p=0}^{P-1} \eta_p \left(\widetilde{\boldsymbol{\gamma}}_p^{(0)} \otimes \cdots \otimes \widetilde{\boldsymbol{\gamma}}_p^{(N-1)}\right), \tag{68}$$

where $\widetilde{\gamma}_{p,d}^{(i)} = \widetilde{\gamma}_{d_i}(f_{p,i}, W_i, I_i)$ *are the one-dimensional approximate basis coefficients defined in* (29). *Additionally, resolution factors* r_i *can be used to improve the approximation.*

Proof. See Appendix B □

The band-limiting region W (51) and the index set I (60) of the channel model (47) fulfill the prerequisites of Theorem 3 with

$$\begin{aligned} W_{0,0} &= 0, \quad W_{\max,0} = \nu_{\mathrm{Dmax}}, \quad M_{0,0} = 0, \quad M_0 = M, \\ W_{0,1} &= W_{\max,1} = \frac{\theta_{\max}}{2}, \quad M_{0,1} = -\left\lfloor \frac{Q}{2} \right\rfloor, \quad M_1 = Q, \\ W_{0,2} &= \frac{\zeta_{\max} + \zeta_{\min}}{2}, \quad W_{\max,2} = \frac{\zeta_{\max} - \zeta_{\min}}{2}, \\ M_{0,2} &= 0, \quad M_2 = N_{\mathrm{Tx}}, \\ W_{0,3} &= \frac{\xi_{\max} + \xi_{\min}}{2}, \quad W_{\max,3} = \frac{\xi_{\max} - \xi_{\min}}{2}, \\ M_{0,3} &= 0, \quad M_3 = N_{\mathrm{Rx}}. \end{aligned} \tag{69}$$

Thus, Theorem 3 allows us to use the methods of Section 3.1 to calculate the basis coefficients of the multidimensional DPS subspace representation approximately with low complexity. The resolution factors r_i, $i = 0, \ldots, N-1$, have to be chosen such that the bias of the subspace representation is small compared to the machine precision $E_{\max}$ of the underlying simulation hardware. A necessary but not sufficient condition for this is to use the methods of Section 3.2 for each dimension independently, that is, to choose $r_i = 2W_{\max,i}/E_{\max}$. However, it has to be verified numerically that the multidimensional DPS subspace representation achieves the required numerical accuracy.

4.4. Complexity and memory requirements

In this subsection, we evaluate the complexity and memory requirements of the N-dimensional SoCE algorithm and the N-dimensional approximate DPS subspace representation, given by Theorem 3. These results are a generalization of the results of Section 3.3. We assume that the one-dimensional DPS sequences $\mathbf{v}^{(d_i)}(W_i, I_i)$, $i = 0, \ldots, N-1$, have been precalculated. Further, we assume that $D = D_0 \cdots D_{N-1}$, where $D_i = \max d_i$ is the maximum number of one-dimensional DPS vectors in dimension i needed to construct the N-dimensional vectors $\mathbf{v}^{(d)}(W, I)$, $d = 0, \ldots, D-1$.

Let the number of operations that are needed to evaluate $\mathbf{h}$ (47) and $\widetilde{\mathbf{h}}^D$ (67) be denoted by $C_{\mathbf{h}}$ and $C_{\widetilde{\mathbf{h}}^D}$, respectively. For the SoCE algorithm,

$$C_{\mathbf{h}} = |I|P(\mathrm{CE} + \mathrm{CM}). \tag{70}$$

For the approximate DPS subspace representation with dimension D, firstly the N-dimensional DPS basis vectors need to be calculated from the one-dimensional DPS vectors (cf. (66)), requiring

$$C_{\mathbf{V}} = (N-1)|I|D\ \mathrm{CM}. \tag{71}$$

Secondly, the approximate basis coefficients $\widetilde{\boldsymbol{\alpha}}$ have to be evaluated according to (68), requiring

$$C_{\widetilde{\boldsymbol{\alpha}}} = \left(\sum_{i=0}^{N-1} |D_i|(\mathrm{CE} + \mathrm{CM} + \mathrm{MA}) + ND\ \mathrm{CM}\right)P. \tag{72}$$

In total, for the evaluation of the approximate subspace representation (67),

$$C_{\widetilde{\mathbf{h}}^D} = |I|D(\mathrm{CM} + \mathrm{MA}) + C_{\mathbf{V}} + C_{\widetilde{\boldsymbol{\alpha}}} \tag{73}$$

operations are required.

Asymptotically for $P \to \infty$, the N-dimensional DPS subspace representation reduces the number of arithmetic operations compared to the SoCE algorithm by the factor

$$\frac{C_{\mathbf{h}}}{C_{\widetilde{\mathbf{h}}}} \longrightarrow \frac{|I|(\mathrm{CE} + \mathrm{CM})}{\sum_{i=0}^{N-1} D_i(\mathrm{CE} + \mathrm{CM}) + ND\ \mathrm{CM}}. \tag{74}$$

The memory requirements of the DPS subspace representation are determined by the size of the index set I, the number of DPS vectors D_i, and the resolution factors r_i. If the DPS sequences are stored with 16-bit precision,

$$\mathrm{Mem}_{\widetilde{\mathbf{h}}} = \sum_{i=0}^{N-1} 2r_i |I_i| D_i\ \mathrm{byte} \tag{75}$$

are needed.

4.5. Numerical examples

Section 3 demonstrated that an application of the approximate DPS subspace representation to the time-domain of wireless channels may save more than an order of magnitude in complexity. In this subsection, the multidimensional approximate DPS subspace representation is applied to an example of a time-variant frequency-selective channel as well as an example of a time-variant frequency-selective MIMO channel. A comparison of the arithmetic complexity is given. We assume a 14-bit fixed-point hardware architecture, that is, a maximum allowable square error of $E_{\max}^2 = (2^{-13})^2 \approx 1.5 \times 10^{-8}$.

Table 2: Simulation parameters for the numerical experiments in the frequency domain.

Parameter	Value
Width of frequency bin F_S	15 kHz
Number of frequency bins Q	256
Maximum delay $\tau_{\max}$	3.7 μs
Maximum norm. delay $\theta_{\max}$	$\approx 1/18$

4.5.1. Time and frequency domain

Table 2 contains the simulation parameters of the numerical experiments in the frequency domain. The parameters in the time domain are chosen according to Table 1. We assume a typical urban environment with a maximum delay spread of $\tau_{\max} = 3.7$ milliseconds given by the ITU Pedestrian B channel model [27].

By omitting the spatial domains $\mathbf{x}$ and $\mathbf{y}$ in (47), we obtain a time-variant frequency-selective GCM

$$h_{\mathbf{m}'} = \sum_{p=0}^{P-1} \eta_p e^{j2\pi\langle \mathbf{f}'_p, \mathbf{m}'\rangle}, \tag{76}$$

where $\mathbf{m}' = [m, q]^T$ and $\mathbf{f}'_p = [\nu_p, \theta_p]^T$. Since (76) is band-limited to

$$W' = [-\nu_{\mathrm{Dmax}}, \nu_{\mathrm{Dmax}}] \times [0, \theta_{\max}] \tag{77}$$

and we wish to calculate (76) in the index set

$$I' = \{0, \ldots, M-1\} \times \left\{ -\left\lfloor \frac{Q}{2} \right\rfloor, \ldots, \left\lfloor \frac{Q}{2} \right\rfloor - 1 \right\}, \tag{78}$$

we can apply a two-dimensional DPS subspace representation (Definition 6) to (76). Further, we can use Theorem 3 to calculate the basis coefficients $\boldsymbol{\alpha}$ of the subspace representation.

For a given maximum allowable square bias $E^2_{\max} = (2^{-13})^2$, the estimated values of the resolution factors in the time and frequency domain are $r_0 = 2\nu_{\mathrm{Dmax}}/E_{\max} \approx 2$ and $r_1 = \theta_{\max}/E_{\max} \approx 512$ (rounded to the next power of two). The square bias

$$\mathrm{bias}^2_{\tilde{\mathbf{h}}^D} = \mathcal{E}\left\{ \frac{1}{MQ} ||\tilde{\tilde{\mathbf{h}}}^D - \mathbf{h}^D||^2 \right\} \tag{79}$$

of the two-dimensional exact and the approximate DPS subspace representation is plotted in Figure 10 against the subspace dimension D. It can be seen that $\mathrm{bias}^2_{\tilde{\mathbf{h}}^D} \approx E^2_{\max}$ at a subspace dimension of approximately $D = 80$. The maximum number of one-dimensional DPS vectors is $D_0 = 4$ and $D_1 = 23$.

4.5.2. Time, frequency, and spatial domain

Table 3 contains the simulation parameters of the numerical experiments in the spatial domain. The remaining parameters are chosen according to Tables 1 and 2. We assume uniform linear arrays at the transmitter and the receiver with

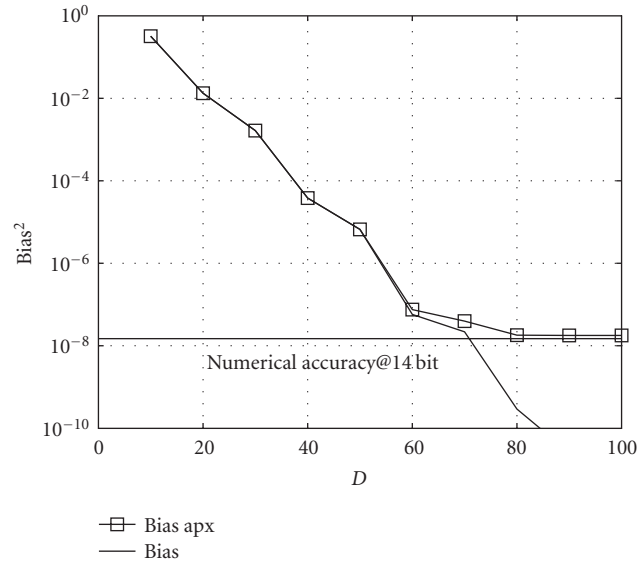

Figure 10: $\mathrm{bias}^2_{\tilde{\mathbf{h}}^D}$ for the subspace representation in the time and frequency domain with $\nu_{\mathrm{Dmax}} = 4.82 \times 10^{-5}$, $M = 2560$, $\theta_{\max} = 0.056$, and $Q = 256$. The resolution factors are fixed to $r_0 = 2$ and $r_1 = 512$. The thin horizontal line denotes the numerical accuracy of a fixed-point 14-bit processor.

Table 3: Simulation parameters for the numerical experiments in the spatial domains.

Parameter	Value
Spacing between antennas D_S	$\lambda/2$ m
Number of Tx antennas N_{Tx}	8
Number of Rx antennas N_{Rx}	8
AoD interval $[\varphi_{\min}, \varphi_{\max}]$	$[-5°, 5°]$
AoA interval $[\psi_{\min}, \psi_{\max}]$	$[-5°, 5°]$
Normalized AoD bandwidth $\zeta_{\max} - \zeta_{\min}$	0.087
Normalized AoA bandwidth $\xi_{\max} - \xi_{\min}$	0.087

spacing $D_S = \lambda/2$ and $N_{\mathrm{Tx}} = N_{\mathrm{Rx}} = 8$ antennas each. Further we assume that there is only one cluster of scatterers in the scenario which is not in the vicinity of the transmitter or receiver (see Figure 11) and we assume no line-of-sight component. The AoD and AoA are assumed to be limited by $[\varphi_{\min}, \varphi_{\max}] = [\psi_{\min}, \psi_{\max}] = [-5°, 5°]$, which has been observed in measurements [32].

A four-dimensional DPS subspace representation is applied to the channel transfer function (47) with W and I defined in (51) and (60). Following the same procedure as in the previous subsection, for a numerical accuracy of 14 bits the estimated values of the resolution factors and the number of one-dimensional DPS vectors in the spatial domains are $r_2 = (\zeta_{\max} - \zeta_{\min})/E_{\max} \approx 512$, $r_3 = (\xi_{\max} - \xi_{\min})/E_{\max} \approx 512$ (rounded to the next power of 2), and $D_2 = D_3 = 5$.

4.5.3. Hybrid DPS subspace representation

Last but not least, we propose a hybrid DPS subspace representation that applies a DPS subspace representation in time

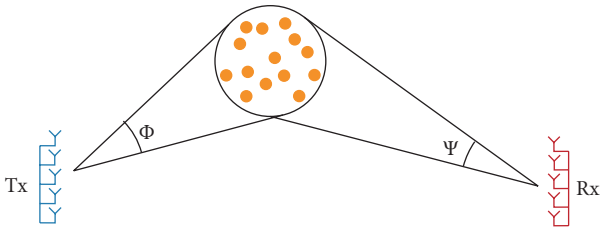

FIGURE 11: Scenario of a mobile radio channel with one cluster of scatterers. The AoD and the AoA are limited within the intervals $\Phi = [\varphi_{\min}, \varphi_{\max}]$ and $\Psi = [\psi_{\min}, \psi_{\max}]$, respectively.

and frequency domains, and computes the complex exponentials in the spatial domain directly. Therefore, the four-dimensional channel transfer function $h_{\mathbf{m}}$ (47) is split into $N_{\mathrm{Tx}}N_{\mathrm{Rx}}$ two-dimensional transfer functions $h^{s,r}_{\mathbf{m}'}$ describing the transfer function between transmit antenna s and receiver antenna r;

$$h^{s,r}_{\mathbf{m}'} := h_{\mathbf{m}',s,r} = \sum_{p=0}^{P-1} \underbrace{\eta_p e^{-j2\pi\zeta_p s} e^{j2\pi\xi_p r}}_{\eta_p^{k,l}} e^{j2\pi\langle \mathbf{f}'_p, \mathbf{m}'\rangle} \quad \text{for } \mathbf{m}' \in I',\ \mathbf{f}'_p \in W', \tag{80}$$

where the band-limit region W' and the index set I' are the same as in the two-dimensional case (cf. (77) and (78)). Then, the two-dimensional DPS subspace representation can be applied to each $h^{s,r}_{\mathbf{m}'}$, $s = 0, \ldots, N_{\mathrm{Tx}} - 1$, $r = 0, \ldots, N_{\mathrm{Rx}} - 1$, independently.

4.5.4. Results and discussion

A complexity comparison of the SoCE algorithm and the approximate DPS subspace representation for one, two, and four dimensions is given in Figure 12. It was evaluated using (70) and (73). Also shown is the complexity of the four-dimensional hybrid DPS subspace representation. It can be seen that for time-variant frequency-flat SISO channels, the one-dimensional DPS subspace representation requires fewer arithmetic operations for $P > 2$ MPCs. The more MPCs are used in the GCM, the more complexity is saved. Asymptotically, the number of arithmetic operations is reduced by $C_{\mathbf{h}}/C_{\tilde{\mathbf{h}}} \to 465$.

For time-variant frequency-selective SISO channels, the two-dimensional DPS subspace representation requires fewer arithmetic operations for $P > 30$ MPCs. However, as noted in Section 4.1, channel models for systems with the given parameters require $P = 400$ paths or more. For such a scenario, the DPS subspace representation saves two orders of magnitude in complexity. Asymptotically, the number of arithmetic operations is reduced by a factor of $C_{\mathbf{h}}/C_{\tilde{\mathbf{h}}} \to 6.8 \times 10^3$ (cf. (74)). The memory requirements are $\mathrm{Mem}_{\tilde{\mathbf{h}}} = 5.83$ Mbyte (cf. (75)).

For time-variant frequency-selective MIMO channels, the four-dimensional DPS subspace representation requires fewer arithmetic operations for $P > 2 \times 10^3$ MPCs. Since MIMO channels require the simulation of up to 10^4 MPCs

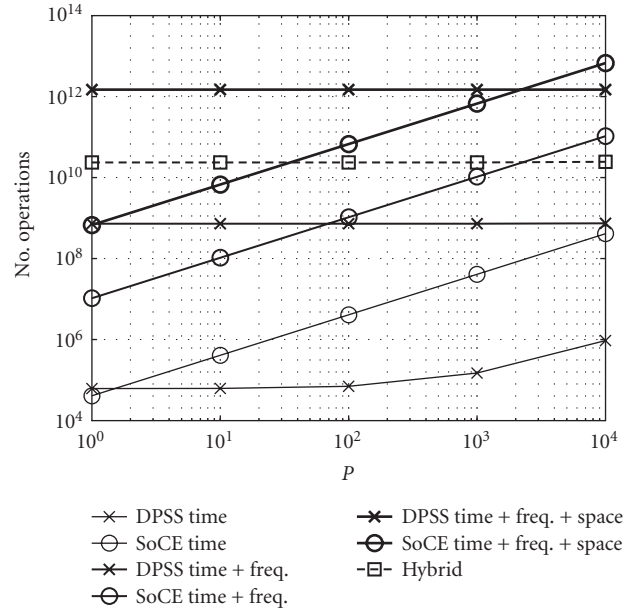

FIGURE 12: Complexity in terms of number of arithmetic operations versus the number of MPCs P. We show results for the SoCE algorithm (denoted by "SoCE") and the approximate DPS subspace representation (denoted by "DPSS") for one, two, and four dimensions. Also shown is the complexity of the four-dimensional hybrid DPS subspace representation (denoted by "Hybrid").

(cf. Section 4.1), complexity savings are still possible. The asymptotic complexity savings are $C_{\mathbf{h}}/C_{\tilde{\mathbf{h}}} \to 1.9 \times 10^4$. However, in the region $P < 2 \times 10^3$ MPCs, the four-dimensional DPS subspace representation requires more complex operations than the corresponding SoCE algorithm. Thus, even though we choose a "best case" scenario with only one cluster, a small angular spread and a low numerical accuracy, there is hardly any additional complexity reduction if the DPS subspace representation is applied in the spatial domain.

The hybrid DPS subspace representation on the other hand exploits the savings of the DPS subspace representation in the time and frequency domain only. From Figure 12 it can be seen that it has fewer arithmetic operations than the four-dimensional DPS subspace representation and the four-dimensional SoCE algorithm for $60 < P < 2 \times 10^3$ MPCs. Thus the hybrid method is preferable for channel simulations in this region. Further, this method also allows for an efficient parallelization on hardware channel simulators [33].

5. CONCLUSIONS

We have presented a low-complexity algorithm for the computer simulation of geometry-based MIMO channel models. The algorithm exploits the low-dimensional subspace spanned by multidimensional DPS sequences. By adjusting the dimension of the subspace, it is possible to trade computational complexity for accuracy. Thus the algorithm is ideally suited for fixed-point hardware architectures with limited precision.

We demonstrated that the complexity reduction depends mainly on the normalized bandwidth of the underlying fading process in time, frequency, and space. If the bandwidth is very small compared to the sampling rate, the essential subspace dimension of the process is small and the complexity can be reduced substantially. In the time domain, the maximum Doppler bandwidth of the fading process is much smaller than the system sampling rate. Compared with the SoCE algorithm, our new algorithm reduces the complexity by more than one order of magnitude on 14-bit hardware.

The bandwidth of a frequency-selective fading process is given by the maximum delay in the channel, which is a factor of five to ten smaller than the sampling rate in frequency. Therefore, the DPS subspace representation also reduces the computational complexity when applied in the frequency domain. To achieve a satisfactory numerical accuracy, the resolution factor in the approximation of the basis coefficients needs to be large, resulting in high memory requirements. On the other hand, it was shown that the number of memory access operations is small. Since this figure has more influence on the run-time of the algorithm, the approximate DPS subspace representation is preferable over the SoCE algorithm for a frequency-selective fading-process.

The bandwidth of the fading process in the spatial domain is determined by the angular spread of the channel, which is almost as large as the spatial sampling rate for most scenarios in wireless communications. Therefore, applying the DPS subspace representation in the spatial domain does not achieve any additional complexity reduction for the scenarios of interest. As a consequence, for the purpose of wideband MIMO channel simulation, we propose to use a hybrid method which computes the complex exponentials in the spatial domain directly and applies the subspace representation to the time and frequency domain only. This method also allows for an efficient parallelization on hardware channel simulators.

APPENDICES

A. CALCULATION OF MULTIDIMENSIONAL DPS SEQUENCES

In the one-dimensional case ($N = 1$), where $W = [W_0 - W_{\max}, W_0 + W_{\max}]$ and $I = \{M_0, \ldots, M_0 + M - 1\}$, the DPS sequences can be calculated efficiently [17, 20]. The efficient and numerically stable calculation of multidimensional DPS sequences with arbitrary W and I is not trivial and has not been treated satisfactorily in the literature. In this section a new way of calculating multidimensional DPS sequences is derived if their passband region can be written as a Cartesian product of one-dimensional intervals.

Indexing every element $\mathbf{m} \in I$ lexicographically, such that $I = \{\mathbf{m}_l, l = 0, 1, \ldots, L-1\}$, we define the matrix $\mathbf{K}^{(W)}$ by

$$K_{k,l}^{(W)} = K^{(W)}(\mathbf{m}_k - \mathbf{m}_l), \quad k, l = 0, \ldots, L-1, \tag{A.1}$$

where the kernel $K^{(W)}$ is given by (55). Let $\mathbf{v}^{(d)}(W, I)$ and $\lambda_d(W, I)$, $d = 0, \ldots, L-1$, denote the eigenvectors and eigenvalues of $\mathbf{K}^{(W)}$:

$$\mathbf{K}^{(W)}\mathbf{v}^{(d)}(W, I) = \lambda_d(W, I)\mathbf{v}^{(d)}(W, I), \tag{A.2}$$

where

$$\lambda_0(W, I) \geq \lambda_1(W, I) \geq \cdots \geq \lambda_{L-1}(W, I). \tag{A.3}$$

It can be shown that the eigenvectors $\mathbf{v}^{(d)}(W, I)$ and the eigenvalues $\lambda_d(W, I)$ are exactly the multidimensional DPS vectors defined in (57) and their corresponding eigenvalues. If the DPS sequences are required for $\mathbf{m} \notin I$, they can be extended using (54).

The multidimensional DPS vectors can theoretically be calculated for an arbitrary passband region W directly from the eigenproblem (A.2). However, since the matrix $\mathbf{K}^{(W)}$ has an exponentially decaying eigenvalue distribution, this method is numerically unstable.

If W can be written as a Cartesian product of one-dimensional intervals (i.e., W is a hyper-cube),

$$W = W_0 \times \cdots \times W_{N-1}, \tag{A.4}$$

where $W_i = [W_{0,i} - W_{\max,i}, W_{0,i} + W_{\max,i}]$, and the index-set I is written as

$$I = I_0 \times \cdots \times I_{N-1}, \tag{A.5}$$

where $I_i = \{M_{0,i}, \ldots, M_{0,i} + M_i - 1\}$, the defining kernel $K^{(W)}$ for the multidimensional DPS vectors evaluates to

$$\begin{aligned} K^{(W)}(\mathbf{u}) &= \int_{W_{0,i}-W_{\max,i}}^{W_{0,i}+W_{\max,i}} \cdots \int_{W_{0,N-1}-W_{\max,N-1}}^{W_{0,N-1}+W_{\max,N-1}} e^{2\pi j f_0'' u_0} \\ &\quad \cdots e^{2\pi j f_{N-1}'' u_{N-1}} df_0'' \cdots df_{N-1}'' \\ &= \prod_{i=0}^{N-1} K^{(W_i)}(u_i), \end{aligned} \tag{A.6}$$

where $\mathbf{u} = [u_0, \ldots, u_{N-1}]^T \in I$. This means that the kernel $K^{(W)}$ is separable and thus the matrix $\mathbf{K}^{(W)}$ can be written as a Kronecker product

$$\mathbf{K}^{(W)} = \mathbf{K}^{(W_0)} \otimes \cdots \otimes \mathbf{K}^{(W_{N-1})}, \tag{A.7}$$

where $\mathbf{K}^{(W_i)}$, $i = 0, \ldots, N-1$, are the kernel matrices corresponding to the one-dimensional DPS vectors. Now let $\lambda_{d_i}(W_i, I_i)$ and $\mathbf{v}^{(d_i)}(W_i, I_i)$, $d_i = 0, \ldots, M_i - 1$, denote the eigenvalues and the eigenvectors of $\mathbf{K}^{(W_i)}$, $i = 0, \ldots, N-1$, respectively. Then the eigenvalues of $\mathbf{K}^{(W)}$ are given by [34, Chapter 9]

$$\begin{aligned} \lambda_{\mathbf{d}}(W, I) &= \lambda_{d_0}(W_0, I_0) \cdots \lambda_{d_{N-1}}(W_{N-1}, I_{N-1}), \\ &\quad d_i = 0, \ldots, M_i - 1,\ i = 0, \ldots, N-1 \end{aligned} \tag{A.8}$$

and the corresponding eigenvectors are given by

$$\mathbf{v}^{(\mathbf{d})}(W,I) = \mathbf{v}^{(d_0)}(W_0,I_0) \otimes \cdots \otimes \mathbf{v}^{(d_{N-1})}(W_{N-1},I_{N-1}),$$
$$d_i = 0,\ldots,M_i-1,\ i=0,\ldots,N-1. \tag{A.9}$$

The eigenvalues $\lambda_{\mathbf{d}}(W,I)$ and the eigenvectors $\mathbf{v}^{(\mathbf{d})}(W,I)$ are index by $\mathbf{d} = [d_0,\ldots,d_{N-1}]^T \in I$. The multidimensional DPS vectors $\mathbf{v}^{(d)}(W,I)$ are obtained by reordering the eigenvectors $\mathbf{v}^{(\mathbf{d})}(W,I)$ and eigenvalues $\lambda_{\mathbf{d}}(W,I)$ according to (A.3). Therefore, we define the mapping $d = \sigma(\mathbf{d})$, such that $\lambda_d(W,I) = \lambda_{\sigma(\mathbf{d})}(W,I)$ is the dth largest eigenvalue. Further define the inverse mapping $\mathbf{d} = \delta(d) = \sigma^{-1}(d)$, such that for a given order d of the multidimensional DPS vector $\mathbf{v}^{(d)}(W,I)$, the corresponding one-dimensional DPS vectors can be found. When a certain multidimensional DPS sequence of a given order d is needed, the eigenvalues λ_d, $d = 0,\ldots,L-1$, have to be calculated and sorted first. Then the one-dimensional DPS sequences corresponding to $\mathbf{d} = \delta(d)$ can be selected.

B. PROOF OF THEOREM 3

For I given by (65), $\mathbf{h}$ can be written as

$$\mathbf{h} = \sum_{p=0}^{P-1} \eta_p \left(\mathbf{e}_p^{(0)} \otimes \cdots \otimes \mathbf{e}_p^{(N-1)}\right), \tag{B.1}$$

where $\mathbf{e}_p^{(i)} = [e^{2\pi j f_{p,i} M_{0,i}},\ldots,e^{2\pi j f_{p,i}(M_{0,i}+M_i-1)}]^T$. Further, since W is given by (64), the results of Appendix A can be used and $\mathbf{V}$ can be written as

$$\mathbf{V} = \mathbf{V}_0 \diamond \cdots \diamond \mathbf{V}_{N-1}, \tag{B.2}$$

where every $M_i \times D_i$ matrix $\mathbf{V}_i$ contains the one-dimensional DPS vectors $\mathbf{v}^d(W_i,I_i)$ in its columns.

Using the identity

$$(\mathbf{A}_0 \diamond \cdots \diamond \mathbf{A}_{N-1})(\mathbf{b}_0 \otimes \cdots \otimes \mathbf{b}_{N-1}) = \mathbf{A}_0\mathbf{b}_0 \otimes \cdots \otimes \mathbf{A}_{N-1}\mathbf{b}_{N-1}, \tag{B.3}$$

the basis coefficients $\boldsymbol{\alpha}$ can be calculated by

$$\boldsymbol{\alpha} = \mathbf{V}^H\mathbf{h} = \sum_{p=0}^{P-1} \eta_p \left(\mathbf{V}_0^H \diamond \cdots \diamond \mathbf{V}_{N-1}^H\right)\left(\mathbf{e}_p^{(0)} \otimes \cdots \otimes \mathbf{e}_p^{(N-1)}\right)$$
$$= \sum_{p=0}^{P-1} \eta_p \Big(\underbrace{\mathbf{V}_0^H\mathbf{e}_p^{(0)}}_{=:\boldsymbol{\gamma}_p^{(0)}} \otimes \cdots \otimes \underbrace{\mathbf{V}_{N-1}^H\mathbf{e}_p^{(N-1)}}_{=:\boldsymbol{\gamma}_p^{(N-1)}}\Big). \tag{B.4}$$

C. LIST OF SYMBOLS

t, f, x, y:	Time, frequency, antenna location at transmitter, and antenna location at receiver
$h(t,f,x,y)$:	Channel transfer function
T_S, F_S, D_S:	Duration of a sample, width of a frequency bin, and spacing between antennas
m, q, s, r:	Discrete time index, frequency index, antenna index at transmitter, antenna index at receiver
$h_{m,q,r,s}$:	Sampled channel transfer function
M, Q:	Number of samples in time and frequency
$N_{\mathrm{Tx}}, N_{\mathrm{Rx}}$:	Number of transmit antennas, number of receive antennas
$\mathbf{h}$:	Vector of index-limited transfer function
P:	Number of MPCs
η_p:	Complex path weight
ω_p, ν_p:	Doppler shift and normalized Doppler shift of the pth MPC
$\omega_{\mathrm{Dmax}}, \nu_{\mathrm{Dmax}}$:	Maximum Doppler shift, maximum normalized Doppler shift
τ_p, θ_p:	Delay and normalized delay of the pth MPC
$\tau_{\max}, \theta_{\max}$:	Maximum delay, maximum normalized delay
φ_p, ζ_p:	AoD and normalized AoD of the pth MPC
$\varphi_{\max}, \varphi_{\min}$:	Maximum and minimum AoD
$\zeta_{\max}, \zeta_{\min}$:	Maximum and minimum normalized AoD
ψ_p, ξ_p:	AoA and normalized AoA of the pth MPC
$\psi_{\max}, \psi_{\min}$:	Maximum and minimum AoD
$\xi_{\max}, \xi_{\min}$:	Maximum and minimum normalized AoD
f_C, c:	Carrier frequency, speed of light
$\nu_{\max}$:	Maximum velocity of user
W:	Band-limiting region
I:	Index set
$v_m^{(d)}(W,I)$:	dth one-dimensional DPS sequence
$v_{\mathbf{m}}^{(d)}(W,I)$:	dth multidimensional DPS sequence
$\mathbf{v}(d)(W,I)$:	One-dimensional or multidimensional DPS vector
$\lambda_d(W,I)$:	Eigenvalue of dth DPS sequence
D, D':	Subspace dimension and essential subspace dimension
$U_d(\nu), \widetilde{U}_d(\nu)$:	DPS wave function and approximate DPS wave function
$\alpha_d, \widetilde{\alpha}_d$:	dth basis coefficient and approximate basis coefficient of DPS subspace representation of $\mathbf{h}$

$\gamma_{p,d}$, $\tilde{\gamma}_{p,d}$: dth basis coefficient and approximate basis coefficient of DPS subspace representation of the pth MPC

r_i, D_i: Resolution factor and maximum number of one-dimensional DPS vectors in time ($i = 0$), frequency ($i = 1$), space at the transmitter ($i = 2$), and space at the receiver ($i = 3$)

$E^2_{\max}$: Maximum squared accuracy of hardware

$\text{bias}^2_{\hat{\mathbf{h}}_D}$: Squared bias of the D-dimensional subspace representation of $\mathbf{h}$

$C_{\hat{\mathbf{h}}_D}$: Computational complexity of the D-dimensional subspace representation of $\mathbf{h}$

ACKNOWLEDGMENTS

This work was funded by the Wiener Wissenschafts-, Forschungs- und Technologiefonds (WWTF) in the ftw. project I2 "Future Mobile Communications Systems." The authors would like to thank the anonymous reviewers for their comments, which helped to improve the paper. Part of this work has been presented at the 5th Vienna Symposium on Mathematical Modeling (MATHMOD 2006), Vienna, Austria, February 2006, at the 15th IST Mobile and Wireless Communications Summit, Mykonos, Greece, June 2006, and at the first European Conference on Antennas and Propagation (EuCAP 2006), Nice, France, November 2006, as an invited paper.

REFERENCES

[1] L. M. Correia, Ed., *Mobile Broadband Multimedia Networks Techniques, Models and Tools for 4G*, Elsevier, New York, NY, USA, 2006.

[2] F. Kaltenberger, G. Steinböck, R. Kloibhofer, R. Lieger, and G. Humer, "A multi-band development platform for rapid prototyping of MIMO systems," in *Proceedings of ITG Workshop on Smart Antennas*, pp. 1–8, Duisburg, Germany, April 2005.

[3] J. Kolu and T. Jamsa, "A real-time simulator for MIMO radio channels," in *Proceedings of the 5th International Symposium on Wireless Personal Multimedia Communications (WPMC '02)*, vol. 2, pp. 568–572, Honolulu, Hawaii, USA, October 2002.

[4] Azimuth Systems Inc., "ACE 400NB MIMO channel emulator," Product Brief, 2006, http://www.azimuthsystems.com/files/public/PB_Ace400nb_final.pdf.

[5] Spirent Communications Inc., "SR5500 wireless channel emulator," Data Sheet, 2006, http://www.spirentcom.com/documents/4247.pdf.

[6] T. Zemen and C. F. Mecklenbräuker, "Time-variant channel estimation using discrete prolate spheroidal sequences," *IEEE Transactions on Signal Processing*, vol. 53, no. 9, pp. 3597–3607, 2005.

[7] R. Clarke, "A statistical theory of mobile-radio reception," *The Bell System Technical Journal*, vol. 47, no. 6, pp. 957–1000, 1968.

[8] W. Jakes, *Microwave Mobile Communications*, John Wiley & Sons, New York, NY, USA, 1974.

[9] M. Pätzold and F. Laue, "Statistical properties of Jakes' fading channel simulator," in *Proceedings of the 48th IEEE Vehicular Technology Conference (VTC '98)*, vol. 2, pp. 712–718, Ottawa, Canada, May 1998.

[10] M. F. Pop and N. C. Beaulieu, "Limitations of sum-of-sinusoids fading channel simulators," *IEEE Transactions on Communications*, vol. 49, no. 4, pp. 699–708, 2001.

[11] P. Dent, G. E. Bottomley, and T. Croft, "Jakes fading model revisited," *Electronics Letters*, vol. 29, no. 13, pp. 1162–1163, 1993.

[12] Y. Li and X. Huang, "The simulation of independent Rayleigh faders," *IEEE Transactions on Communications*, vol. 50, no. 9, pp. 1503–1514, 2002.

[13] Y. R. Zheng and C. Xiao, "Simulation models with correct statistical properties for Rayleigh fading channels," *IEEE Transactions on Communications*, vol. 51, no. 6, pp. 920–928, 2003.

[14] A. G. Zajić and G. L. Stüber, "Efficient simulation of Rayleigh fading with enhanced de-correlation properties," *IEEE Transactions on Wireless Communications*, vol. 5, no. 7, pp. 1866–1875, 2006.

[15] T. Zemen, C. Mecklenbräuker, F. Kaltenberger, and B. H. Fleury, "Minimum-energy band-limited predictor with dynamic subspace selection for time-variant flat-fading channels," to appear in *IEEE Transactions on Signal Processing*.

[16] T. Zemen, "OFDM multi-user communication over time-variant channels," Ph.D. dissertation, Vienna University of Technology, Vienna, Austria, July 2004.

[17] D. Slepian, "Prolate spheroidal wave functions, Fourier analysis, and uncertainty—V: the discrete case," *The Bell System Technical Journal*, vol. 57, no. 5, pp. 1371–1430, 1978.

[18] D. J. Thomson, "Spectrum estimation and harmonic analysis," *Proceedings of the IEEE*, vol. 70, no. 9, pp. 1055–1096, 1982.

[19] S. Dharanipragada and K. S. Arun, "Bandlimited extrapolation using time-bandwidth dimension," *IEEE Transactions on Signal Processing*, vol. 45, no. 12, pp. 2951–2966, 1997.

[20] D. B. Percival and A. T. Walden, *Spectral Analysis for Physical Applications*, Cambridge University Press, Cambridge, UK, 1963.

[21] F. Kaltenberger, T. Zemen, and C. W. Ueberhuber, "Low complexity simulation of wireless channels using discrete prolate spheroidal sequences," in *Proceedings of the 5th Vienna International Conference on Mathematical Modelling (MATHMOD '06)*, Vienna, Austria, February 2006.

[22] D. Slepian and H. O. Pollak, "Prolate spheroidal wave functions, Fourier analysis and uncertainty—I," *The Bell System Technical Journal*, vol. 40, no. 1, pp. 43–64, 1961.

[23] A. Papoulis, *Probability, Random Variables and Stochastic Processes*, McGraw-Hill, New York, NY, USA, 3rd edition, 1991.

[24] H. Holma and A. Tskala, Eds., *WCDMA for UMTS*, John Wiley & Sons, New York, NY, USA, 2nd edition, 2002.

[25] M. Steinbauer, A. F. Molisch, and E. Bonek, "The double-directional radio channel," *IEEE Antennas and Propagation Magazine*, vol. 43, no. 4, pp. 51–63, 2001.

[26] P. Almers, E. Bonek, A. Burr, et al., "Survey of channel and radio propagation models for wireless MIMO systems," *EURASIP Journal on Wireless Communications and Networking*, vol. 2007, Article ID 19070, 19 pages, 2007.

[27] Members of 3GPP, "Technical specification group radio access network; User Equipment (UE) radio transmission and reception (FDD)," Tech. Rep. 3GPP TS 25.101 version 6.4.0, 3GPP, Valbonne, France, March 2004.

[28] V. Erceg, L. Schumacher, P. Kyritsi, et al., "TGn channel models," Tech. Rep. IEEE P802.11, Wireless LANs, Garden Grove, Calif, USA, May 2004.
[29] V. Degli-Esposti, F. Fuschini, E. M. Vitucci, and G. Falciasecca, "Measurement and modelling of scattering from buildings," *IEEE Transactions on Antennas and Propagation*, vol. 55, no. 1, pp. 143–153, 2007.
[30] T. Pedersen and B. H. Fleury, "A realistic radio channel model based on stochastic propagation graphs," in *Proceedings of the 5th Vienna International Conference on Mathematical Modelling (MATHMOD '06)*, Vienna, Austria, February 2006.
[31] O. Norklit and J. B. Andersen, "Diffuse channel model and experimental results for array antennas in mobile environments," *IEEE Transactions on Antennas and Propagation*, vol. 46, no. 6, pp. 834–840, 1998.
[32] N. Czink, E. Bonek, X. Yin, and B. Fleury, "Cluster angular spreads in a MIMO indoor propagation environment," in *Proceedings of the 16th International Symposium on Personal, Indoor and Mobile Radio Communications (PIMRC '05)*, vol. 1, pp. 664–668, Berlin, Germany, September 2005.
[33] F. Kaltenberger, G. Steinböck, G. Humer, and T. Zemen, "Low-complexity geometry based MIMO channel emulation," in *Proceedings of European Conference on Antennas and Propagation (EuCAP '06)*, Nice, France, November 2006.
[34] T. K. Moon and W. Stirling, *Mathematical Methods and Algorithms*, Prentice-Hall, Upper Saddle River, NJ, USA, 2000.

Florian Kaltenberger was born in Vienna, Austria, in 1978. He received his Diploma (Dipl.-Ing. degree) and his Ph.D. degree both in technical mathematics from the Vienna University of Technology in 2002 and 2007, respectively. During the summer of 2001, he held an internship position with British Telecom, BT Exact Technologies in Ipswich, UK, where he was working on mobile video conferencing applications. After his studies, he started as a Research Assistant at the Vienna University of Technology, Institute for Advanced Scientific Computing, working on distributed signal processing algorithms. In 2003, he joined the wireless communications group at the Austrian Research Centers GmbH, where he is currently working on the development of low-complexity smart antenna and MIMO algorithms as well as on the ARC SmartSim real-time hardware channel simulator. His research interests include signal processing for wireless communications, MIMO communication systems, receiver design and implementation, MIMO channel modeling and simulation, and hardware implementation issues.

Thomas Zemen was born in Mödling, Austria, in 1970. He received the Dipl.-Ing. degree (with distinction) in electrical engineering from Vienna University of Technology in 1998 and the Ph.D. degree (with distinction) in 2004. He joined Siemens Austria in 1998, where he worked as Hardware Engineer and Project Manager for the radio communication devices department. He was engaged in the development of a vehicular GSM telephone system for a German car manufacturer. From October 2001 to September 2003, Mr. Zemen was delegated by Siemens Austria as a Researcher to the mobile communications group at the Telecommunications Research Center Vienna (ftw.). Since October 2003, Thomas Zemen has been with the Telecommunications Research Center, Vienna, working as a Researcher in the strategic I0 project. His research interests include orthogonal frequency division multiplexing (OFDM), multiuser detection, time-variant channel estimation, iterative MIMO receiver structures, and distributed signal processing. Since May 2005, Thomas Zemen leads the project "Future Mobile Communications Systems-Mathematical Modeling, Analysis, and Algorithms for Multi Antenna Systems" which is funded by the Vienna Science and Technology Fund (Wiener Wissenschafts-, Forschungs- und Technologiefonds—WWTF). Dr. Zemen teaches "MIMO Communications" as external lecturer at Vienna University of Technology.

Christoph W. Ueberhuber received the Dipl.-Ing. and Ph.D. degrees in technical mathematics and the Venia Docendi Habilitation degree in numerical mathematics from the Vienna University of Technology, Vienna, Austria, in 1973, 1976, and 1979, respectively. He has been with the Vienna University of Technology since 1973 and is currently a Professor of numerical mathematics. He has published 15 books and more than 100 papers in journals, books, and conference proceedings. His research interests include numerical analysis, high-performance numerical computing, and advanced scientific computing.